THE JOURNAL OF BIOLOGICAL CHEMISTRY
Vol. 277, No. 10, Issue of March 8, pp. 8524–8530, 2002
Printed in U.S.A.

Structure of Human NMN Adenylyltransferase

A KEY NUCLEAR ENZYME FOR NAD HOMEOSTASIS*

Received for publication, December 5, 2001, and in revised form, December 19, 2001
Published, JBC Papers in Press, December 19, 2001, DOI 10.1074/jbc.M111589200

Silvia Garavaglia‡, Igor D'Angelo‡, Monica Emanuelli§, Francesco Carnevali§, Francesca Pierella§, Giulio Magni§¶, and Menico Rizzi‡‖**

From the ‡Department of Genetics and Microbiology "A. Buzzati Traverso," University of Pavia, Via Ferrata 1, 27100 Pavia, Italy, §Institute of Biochemistry, University of Ancona, via Ranieri, 60131 Ancona, Italy, and ‖DISCAFF, University of Piemonte Orientale "Amedeo Avogadro," Viale Ferrucci 33, 28100 Novara, Italy

Nicotinamide mononucleotide adenylyltransferase (NMNAT), a member of the nucleotidyltransferase α/β-phosphodiesterases superfamily, catalyzes a universal step (NMN + ATP = NAD + PP_i) in NAD biosynthesis. Localized within the nucleus, the activity of the human enzyme is greatly altered in tumor cells, rendering it a promising target for cancer chemotherapy. By using a combination of single isomorphous replacement and density modification techniques, the human NMNAT structure was solved by x-ray crystallography to a 2.5-Å resolution, revealing a hexamer that is composed of α/β-topology subunits. The active site topology of the enzyme, analyzed through homology modeling and structural comparison with other NMNATs, yielded convincing evidence for a substrate-induced conformational change. We also observed remarkable structural conservation in the ATP-recognition motifs G*XXX*P*X*-(T/H)*XX*H and S*XT XXR*, which we take to be the universal signature for NMNATs. Structural comparison of human and prokaryotic NMNATs may also lead to the rational design of highly selective antimicrobial drugs.

Beyond its pivotal role as a redox cofactor in energy transduction and cellular metabolism, NAD is also intimately involved in signaling pathways. The NAD(P) derivatives nicotinic acid adenine dinucleotide phosphate and cyclic ADP-ribose are likewise among the most potent calcium-mobilizing agents (1, 2). NAD is the substrate for poly(ADP-ribosyl)ation, a vitally important post-translation modification occurring within the nuclei of higher eukaryotes by poly(ADP-ribose) polymerase (3). NAD is also the substrate for mono-ADP-ribosyltransferase, an enzyme that transfers a single ADP-ribose unit from NAD onto target proteins in both mammalian and prokaryotic cells (4). Most recently, high levels of NAD were shown to extend yeast cell life-span, a phenomenon linked to the action of NAD-dependent catalysis of protein deacetylation (5, 6).

Like ATP and GTP, NAD performs multiple tasks in both energy and signaling transduction, indicating why NAD homeostasis must be tightly regulated in all living organisms. Any impairment in NAD synthesis seriously impairs cellular metabolism, eventually resulting in cell death (7). The biosynthesis of this key redox coenzyme is accomplished either through a *de novo* pathway or through NAD-recycling salvage routes with notable differences between prokaryotes and eukaryotes (8). All the known biochemical pathways converge to the reaction catalyzed by NMN adenylyltransferase (EC 2.7.7.1), abbreviated NMNAT[1] (8). This transferase catalyzes the nucleophilic attack by the 5′ phosphate NMN or nicotinic acid mononucleotide on the α-phosphoryl of ATP, releasing PP_i and NAD or nicotinic acid adenine dinucleotide (9). Although the eukaryotic enzyme forms NAD and nicotinic acid adenine dinucleotide at similar rates, its prokaryotic counterpart prefers the deamidated substrate (nicotinic acid mononucleotide) (8). Because the reaction is fully reversible, NAD can also be reconverted to ATP (10).

Human NMNAT, the only NAD/nicotinic acid adenine dinucleotide biosynthetic-pathway enzyme within the nucleus (11, 12), may be so localized to meet the consistently high demand for NAD in nuclear poly(ADP-ribosyl)ation reactions. A critical factor in cell survival, NMNAT activity is altered in highly proliferating cells, rendering the enzyme a potential target for cancer chemotherapy (13, 14). An equally relevant issue is the multistep metabolic activation of the prodrug tiazofurin (15) to form tiazofurin adenine dinucleotide where the last step is mediated by NMNAT. The NAD analog known as tiazofurin adenine dinucleotide strongly inhibits IMP dehydrogenase, a widely acknowledged target for cancer chemotherapy (16). NMNAT activity is reduced to below 5% of its wild type activity in a tiazofurin-resistant cell line (17), stressing the key role of NMNAT both in prodrug activation and as a potential target for cancer chemotherapy.

Because our group aspires to achieve the rational design of antineoplastic and antimicrobial agents (18, 21, 22), the crystallographic investigation reported here provides the first opportunity to compare the detailed structures of human and prokaryotic NMN adenylyltransferases. Based on structural similarities identified on the basis of the *Methanococcus jann-*

* This research was supported in part by grants from Ministero dell'Università e della Ricerca Scientifica e Tecnologica (Project 'Studi strutturali sulla L-aspartato ossidasi, NMN adeniltransferasi e NAD sintetasi'), Consiglio Nazionale delle Ricerche (Target Project "Biotechnology"), and the Agenzia Spaziale Italiana (Project number I/R/67/01). The costs of publication of this article were defrayed in part by the payment of page charges. This article must therefore be hereby marked "*advertisement*" in accordance with 18 U.S.C. Section 1734 solely to indicate this fact.

The atomic coordinates and structure factors (code 1KKU) have been deposited in the Protein Data Bank, Research Collaboratory for Structural Bioinformatics, Rutgers University, New Brunswick, NJ (http://www.rcsb.org/).

¶ To whom correspondence may be addressed: Institute of Biochemistry, University of Ancona, Via Ranieri, 60131 Ancona, Italy. Tel.: 39-071-2204678; Fax: 39-071-2802117; E-mail: magnig@mta01.unian.it.

** To whom correspondence may be addressed: Dept. of Genetics and Microbiology, University of Pavia, Via Ferrata 1, 27100 Pavia, Italy. Tel.: 39-0382-505560; Fax: 39-0382-528496; E-mail: rizzi@ipvgen.unipv.it.

[1] The abbreviations used are: NMNAT, nicotinamide mononucleotide adenylyltransferase; SIR, simple isomorphous replacement; r.m.s., root mean square; r.m.s.d., root mean square deviation; PPAT, phosphopantetheine adenylyltransferase.

aschii structure, previously solved by our group (18), NMNAT was recognized to be a member of the nucleotidyltransferase superfamily of α/β-phosphodiesterases. Characterized by the presence of a highly conserved (H/T)*X*GH motif (19), these enzymes share a common adenylylation mechanism. We have now determined the crystal structure of recombinant human NMN adenylyltransferase in its free form at a resolution of 2.5 Å. The structure reveals a hexameric assembly with 322 symmetry composed of α/β-topology subunits. The enzyme active site has been analyzed through a detailed structural comparison with *M. jannaschii* (18) and *Methanobacterium thermoautotrophicum* NMNATs (20). Our structural data also revealed a remarkable structural conservation in ATP-recognition motifs G*XXX*P*X*(T/H)*XX*H and S*XTXX*R, which we propose to be the universal signature for NMNATs.

EXPERIMENTAL PROCEDURES

Crystallization—The recombinant protein used in the crystallization experiments was purified from *Escherichia coli* as described previously and consists of a polypeptide chain of 279 residues (14). The protein was provided in a buffered solution containing 0.02 M Tris at pH 8.0, 2 mM ATP, and 2 mM $MgCl_2$ and has proven to be active. Crystals of human NMNAT were grown using the hanging drop vapor diffusion method by equilibrating 2 μl of purified protein solution at a concentration of 20 mg/ml against an equal volume of reservoir solution containing 1.8 M ammonium sulfate, 0.1 M Tris, pH 8.1, 4% v/v isopropyl alcohol.

The crystals grow to a size of ~0.1 × 0.1 × 0.1 mm in about 4–5 days at 20 °C and can be assigned to two different space groups depending on the cryoprotectant employed for data collection at 100 K. If 20% glycerol is used, the analysis of the diffraction data sets collected allowed us to assign the NMNAT crystals to the monoclinic space group $P2_1$ (crystal form I) with cell dimensions a = 141.0 Å, b = 87.0 Å, c = 141.9 Å, β = 118.10° containing six molecules per asymmetric unit with a corresponding solvent content of 70%. For crystal form I, a diffraction limit of a 3.3-Å resolution was observed. On the other hand, when light paraffin oil is employed as a cryoprotectant, NMNAT crystals belong to the hexagonal space group $P6_322$ (crystal form II) with cell dimensions $a = b$ = 147.50 Å and c = 61.50 Å and diffract to a 2.5-Å resolution. In this case, one molecule is present per asymmetric unit with a corresponding solvent content of 60%.

Structure Solution and Refinement—For data collection and heavy atom screening, the crystals were transferred in a stabilizing solution containing 2.0 M ammonium sulfate, 0.1 M Tris, pH 8.1, 4% v/v isopropyl alcohol, 2 mM ATP, and 2 mM $MgCl_2$. All data sets were collected using synchrotron radiation at the beam line ID14 EH3 at European Synchrotron Radiation Facility (Grenoble, France, λ = 0.8139 Å) at a temperature of 100 K. Diffraction data sets employed for SIR phasing were collected on the monoclinic crystals, whereas the high resolution data set employed in refinement was collected on the hexagonal crystals. Diffracted intensities were evaluated and integrated using the program MOSFLM (23), whereas the CCP4 suite was used for data reduction (24). Table I gives a summary of the data collection statistics. The mercuric chloride isomorphous difference Patterson map was solved using SHELX-90 (25), and heavy atom parameters were refined using MLPHARE (26); phasing statistics are reported in Table I. The soaking time for the mercuric derivative was 6 h at a concentration of 0.5 mM. The initial SIR electron density map calculated for the monoclinic crystal form did not allow chain tracing, providing only a clear identification of the protein boundaries. The initial SIR phases were then sensibly improved by means of 6-fold density averaging. The presence of a hexamer with 32-point group symmetry in the asymmetric unit was confirmed through the calculation of the self-rotation function, performed using the program AmoRe (27). Five strong peaks located at κ = 119.5, ϕ = 84.1, ψ = 273.2 (4.5 σ over r.m.s.); at κ = 180.0, ϕ = 60.0, ψ = 5.8 (4.2 σ over r.m.s.); at κ = 180.0, ϕ = 6.2, ψ = 180.0 (5.2 σ over r.m.s.); and at κ = 180.1, ϕ = 59.7, ψ = 180.0 (10.2 σ over r.m.s.) were identified. This hexameric arrangement was also consistent with the position of the 12 heavy atom sites located in the difference Patterson. The locations of the non-crystallographic 3- and 2-fold axes were determined with the program GLRF (28), used in the real-space translation function mode (option tfun = 2). The SIR phases were then improved by simultaneous application of 6-fold density averaging, solvent flattening, and histogram matching with phase extension from 5.0 to 3.3 Å, as implemented in the program DM (29). The resulting electron density map was of good quality but allowed a clear tracing of the backbone only, suffering from a limited resolution (3.3 Å). Nevertheless, 80% of the entire protein was traced as a polyalanine model at this stage. This partial structure was employed as a search model for molecular replacement calculation against the hexagonal crystal form. An unambiguous solution for both the cross-rotation and translation functions could be obtained using the program AmoRe (27), therefore providing the operator that relates the coordinates of the monoclinic and hexagonal crystal structures. At this point, a multicrystal density averaging procedure was attempted. An envelope was defined on the basis of the polyalanine model built in the monoclinic structure (covering one monomer), whereas the starting electron density was derived from the initial SIR phases. The calculation was carried out with the program DMMULTI (29), extending the phases for the hexagonal crystal form to a 2.5-Å resolution. The resulting electron density map was of high quality, and an unambiguous tracing, including all the side chains, was performed using the program O (30). Nevertheless, three major breaks were present in the electron density map between residues 1–4, 111–147, and 258–279.

TABLE I
Crystallographic statistics

	Native I	$HgCl_2$	Native II
X-ray data			
Space group	$P2_1$	$P2_1$	$P6_322$
Resolution	3.3	4.3	2.5
Unique reflections	42041	14068	14056
Redundancy	3.2	2.3	8.4
Completeness	96.0	98.7	99.8
R_{merge}[a]	10.4	10.0	7.5
R_{iso}[b]		20.4	
Phasing power[c]		1.28	
R_{cullis}[d]		0.80	
FOM[e]		0.31	
No. of protein atoms			1750
No. of solvent atoms			58
R-factor (%)[f]			23.4
R-free (%)[g]			28.6
r.m.s.d. bond lengths (Å)			0.018
r.m.s.d. bond angles (degrees)			2.0
r.m.s.d. planar 1–4 distance (Å)			0.011

[a] $R_{merge} = \Sigma|Ii - \langle Ii\rangle|/\Sigma\langle Ii\rangle$, where $\langle Ii\rangle$ is the mean value of the ith intensity measurements.

[b] $R_{iso} = \Sigma||F_{PH}| - |F_P||/\Sigma|F_P|$, where F_{PH} and F_P are the derivative and native structure factors, respectively.

[c] Phasing power = $|F_H|/E$, where F_H is the calculated heavy atom structure factors and E is the residual lack of closure.

[d] $R_{cullis} = \Sigma||F_{PH} + F_P| - F_H|/\Sigma|F_{PH} + F_P|$, where F_P, F_{PH}, and F_H are the observed protein, observed derivative, and calculated heavy atom structure factors with the sum over all centric reflections.

[e] $\langle FOM\rangle$ (10.0–3.5 Å) = $\int P(\theta) \exp(\iota\theta)d\theta/\int P(\theta)d\theta$, where P is the probability distribution of the phase angle θ.

[f] R-factor = $\Sigma|F_{obs} - F_{calc}|/\Sigma|F_{obs}|$.

[g] R-free = $\Sigma|F_{obs} - F_{calc}|/\Sigma|F_{obs}|$ (for the selected portion of all data).

Only the hexagonal structure was subjected to refinement because of the highest resolution obtained using these crystals. The crystallographic refinement was carried out at 2.5 Å employing REFMAC (31). A random sample containing 965 reflections (roughly 1% of the total number of reflections) was excluded from the refinement and used for the calculation of the free R-factor (32). The program O was used for manual rebuilding of the model. The initial model (80% of the whole molecule) was subjected to 10 cycles of rigid body refinement in the 15.0–4.0 Å resolution range, lowering the R-factor and the R-free to 39 and 41%, respectively. Subsequently, 50 cycles of REFMAC were performed, observing a drop of the crystallographic R-factor to 34% (free R-factor 36%). An additional 50 cycles of refinement were carried out, obtaining a R-factor and a free R-factor of 26 and 28%, respectively. Solvent molecules were manually added at positions with density > 4σ in the $F_o - F_c$ map, considering only peaks engaged in at least one hydrogen bond with protein atom or solvent atom. A final round of 20 cycles of refinement was carried out on the resulting model until convergence, at an R-factor of 23.4% and R-free of 28.1%.

The current model contains 216 amino acid residues and 58 water molecules. The three major breaks detected after the multicrystal density averaging procedure were still present in the refined electron density map, between residues 1–4, 111–147, and 258–279. These breaks in the electron density were also present in all six subunits of the monoclinic structure. The average B-factors for the 1750 protein atoms and for the 58 ordered water molecules are 58.7 and 56.2 $Å^2$ (54.6 $Å^2$ for

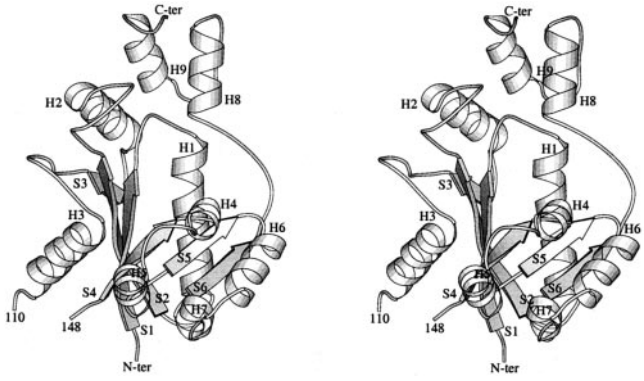

FIG. 1. **Stereo ribbon view of the subunit of human NMN adenylyltransferase, as produced by the program MOLSCRIPT (48).** The parallel central six-stranded β-sheet can be seen roughly edge-on with the topological switch point, representing the NAD binding site.

the main chain and 62.7 Å^2 for the side chains), respectively. The results of refinement are summarized in Table I.

Deposition—The coordinates of human NMNAT have been deposited with the Protein Data Bank (accession code 1KKU).

RESULTS AND DISCUSSION

Overall Quality of the Human NMNAT Structural Model—Two different crystal forms could be obtained depending on the cryocooling condition: crystals of form I belong to the monoclinic space group $P2_1$ with six molecules in the asymmetric unit, and crystals of form II belong to the hexagonal space group $P6_322$ with one molecule in the asymmetric unit (see "Experimental Procedures"). The structure of human NMNAT was solved by means of the single isomorphous replacement method in conjunction with multicrystal density averaging. Only the hexagonal crystal form was refined, and the current model contains 216 residues and 58 solvent molecules with an *R*-factor of 0.234 and *R*-free of 0.286 at a 2.5-Å resolution. No electron density is present for residues 1–4, 111–147, and 258–279, neither in the hexagonal nor in the monoclinic structures. The stereochemistry of the refined model has been assessed with the program PROCHECK (33). 90% of the residues are in the most favored regions of the Ramachandran plot, and no outliers are present. Residue 19 has been recognized as a cis proline. Coordinates of human NMNAT have been deposited with the Protein Data Bank.

Overall Structure—The polypeptide chain of each NMNAT folds into six β-strands, nine α-helices, and connecting loops. The protein architecture consists of a classical α/β-dinucleotide binding domain (residues 5–216) whose core is a strongly twisted six-stranded parallel open β-sheet, flanked on both sides by α-helices (Fig. 1). The C-terminal portion of the protein (residues 217–258) forms a second small domain, made up by two α-helices (Fig. 1). A hexameric assembly was observed in both of the two crystal forms. In the hexagonal crystal form, the 322 crystallographic symmetry operations assemble the monomers present in the asymmetric unit into a hexamer (Fig. 2, *a* and *b*). The same oligomeric arrangement is observed in the monoclinic crystal form, where a hexamer endowed with 32-point group symmetry is present in the asymmetric unit.

The overall quaternary structure can be viewed as a trimer-of-dimers, where two major intersubunit interfaces can be distinguished. The first concerns associated protomers related by a dyad axis (Fig. 2, *a* and *b*), whereas the second involves protomers related by a 3-fold axis (Fig. 2*a*). A total of 2100 Å^2 of molecular surface are buried upon oligomerization on each monomer. In particular, 1200 Å^2 of the accessible surface are buried on each monomer upon dimer formation. Many interactions occurring across the dyad axis participate in dimer stabilization, including hydrogen bonds and hydrophobic contacts. Residues 217–220 meet their equivalent in the facing monomer, and residues 234–238 of one subunit contact residues 26–33 of the other (Fig. 3). Phe-217 appears to play an important role in the dimer stabilization, making a strong hydrophobic interaction with Ile-221 of the other monomer (Fig. 3). Interestingly, a single nucleotide polymorphism was reported for human NMNAT, resulting in the expression of either phenylalanine or leucine at position 217 (34). In our structure, a phenylalanine residue occupies position 217 (Fig. 3). However, the presence of a leucine residue would be fully compatible with the structural environment observed and would not disrupt the network of hydrophobic interaction essential for the dimer stability.

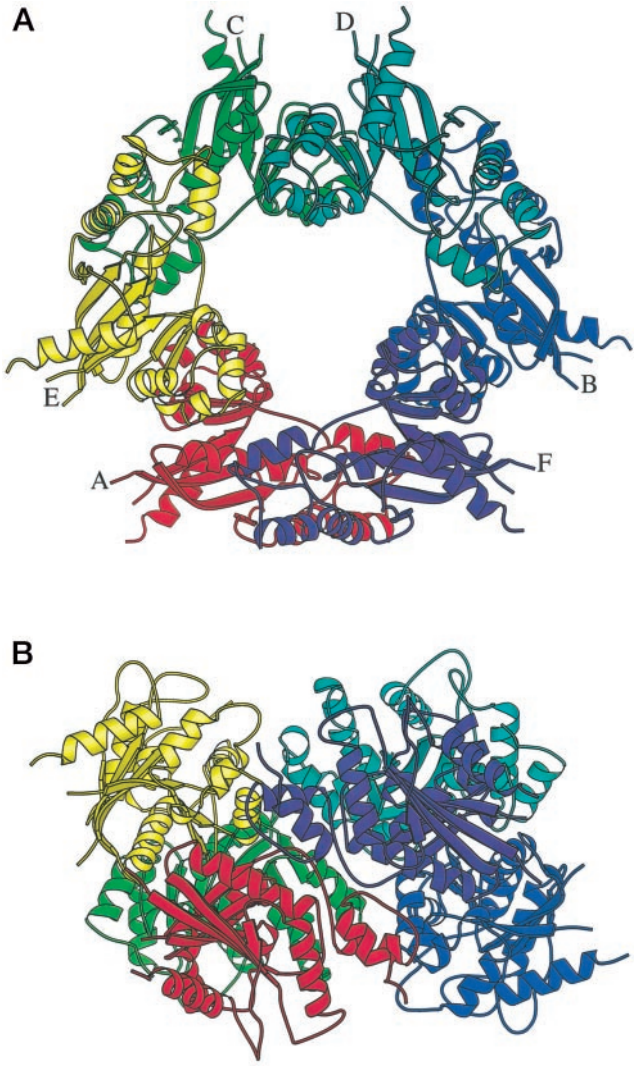

FIG. 2. **Ribbon representation of the hexamer of NMN adenylyltransferase as produced by the program MOLSCRIPT (48) viewed along the local 3-fold axis (*a*) and the local dyad (*b*).** Each of the six subunits is *colored* differently.

Fewer contacts are observed between protomers related by the triad axis where 500 Å^2 of accessible surface area are buried on each monomer upon trimer formation, revealing a loose trimer. The intratrimer contacts observed consist of both electrostatic and hydrophobic interactions and are provided by two regions on each monomer, encompassing residues 198–204 and 228–232. Among the electrostatic interactions observed, Tyr-A198 provides two strong hydrogen bonds with its OH atom at a distance of 2.8 Å from the Arg-B228 NH1 atom and

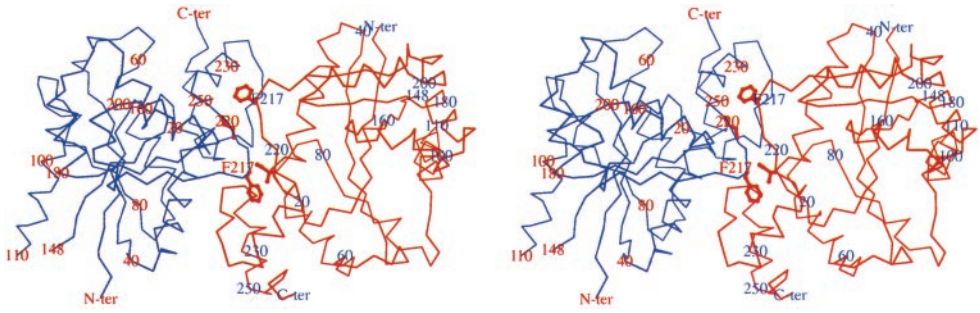

FIG. 3. **Stereo view of the Cα trace of the NMNAT dimer, viewed along its local dyad.** Phe-217 and Ile-221 are shown in a ball-and-stick representation. The figure was generated using MOLSCRIPT (48).

its carbonyl atom at 2.8 Å from the Arg-B231 NH_2 atom. A strong hydrophobic interaction occurs between Trp-B204 and Arg-A232, whose guanidino group stacks against the aromatic ring of Trp-B204. All the contacts observed are repeated between subunit B and C as well as C and A.

The approximate overall dimensions of the globular hexamer of human NMNAT are 60 Å along the triad axis and 50 Å across it. As can be seen in Fig. 2*a*, a solvent channel crosses the entire hexamer running along the 3-fold axis. Based on structural comparison with the previously reported structures *of M. jannaschii* (18) and *M. thermoautotrophicum* (20) NMNAT, we proposed the enzyme active site to be located in a wide cleft facing the channel and extending from the top of the hexamer to the trimer-trimer interface (Fig. 2*a*). The interior of the channel is characterized by a distribution of positively charged residues, including Arg-188, Arg-228, Arg-231, Arg-232, and Lys-225, all located in proximity of the proposed enzyme active site (Fig. 4). As already observed in the hexameric structure of *M. jannaschii* NMNAT, such a distribution could be suited for the highly negative substrate ATP to be steered to its binding site from the bulk solvent (18). However, the extension of the positive surface observed in human NMNAT is smaller than that reported in the case of *M. jannaschii* NMNAT, reflecting the lower number of positively charged residues featuring the active site of the human enzyme (Fig. 4).

The structural arrangement of human NMNAT suggests a conservation of the hexameric assembly in all NMNATs since the same structural architecture was reported for both *M. jannaschii* (18) and *M. thermoautotrophicum* enzymes (20). However, human NMNAT was reported by us to be a tetramer in solution, based on gel filtration experiments (14). Therefore, the crystallographic observed hexamer could not represent the only functionally active oligomeric state for NMNAT. In this respect, the dimer building up the hexamer (Fig. 3) could be considered as the minimal NMNAT oligomeric unit resulting in tetramers or hexamers, depending on the environmental conditions.

Consistent with its subcellular localization, a putative nuclear localization signal was identified in the human enzyme in the ^{123}PGRKRKW^{129} amino acids stretch (12). Moreover, a previously proposed interaction with PARP1 (35) has recently been confirmed (12), stressing a possible role of NMNAT in regulating PARP1 activity. Despite the fact that NMNAT was proven to be a substrate for nuclear kinases *in vitro* (12), either which of the proposed putative residues (positions 109, 136, and 256) is actually phosphorylated or whether the phosphorylated form has a precise physiological role is still unknown (12). However, it is tempting to speculate a possible role of phosphorylation in regulating either the enzyme activity or the interaction with PARP1. In this respect, it should be noticed that both the putative phosphorylation sites and the nuclear localization signal are disordered in our structure (Fig. 1). We speculate that a conformational change may occur upon phosphorylation and/or formation of a protein·protein complex with PARP1, resulting in the structuration of the flexible regions.

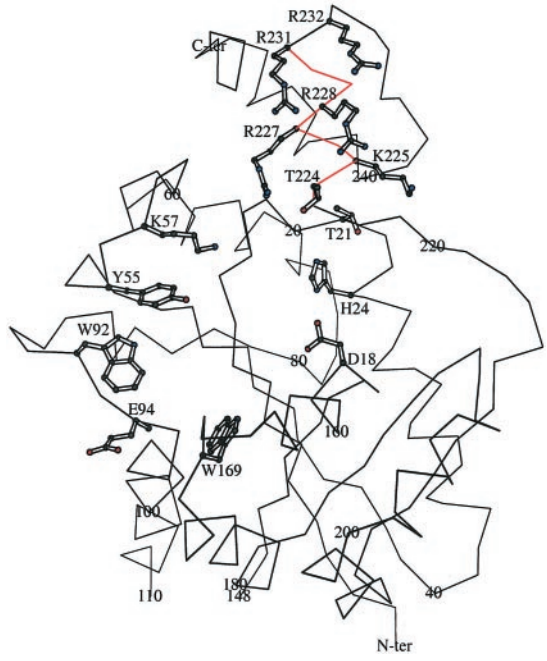

FIG. 4. **Cα trace of the NMNAT subunit.** The residues surrounding the active site are drawn in a ball-and-stick representation. The helix H8 is colored in *red*. The figure was generated using MOLSCRIPT (48).

Comparison of the Active Site of the Human Enzyme with Those of Other NMN Adenylyltransferases—The catalytic mechanism of this key enzyme has been investigated in depth, showing a kinetic behavior fully compatible with an ordered sequential Bi-Bi mechanism (36). According to the proposed mechanism, NMN binds first followed by ATP, and in the reversed reaction, PP_i precedes NAD. Once both NMN and ATP are bound to the active site of the enzyme, the reaction proceeds through a nucleophilic attack by the 5′ phosphate of NMN on the α-phosphoryl of ATP, assisted by a magnesium ion that plays an essential role in catalysis (9, 18).

We cannot presently obtain diffracting crystals of enzyme complexed with any of its substrates. Attempts at enzyme co-crystallization with ATP or NAD invariably yielded crystals of the free form. When co-crystallizations were attempted with NMN or PP_i, no crystals were obtained under conditions that routinely produced crystals of the free form. A possible explanation is the strict substrate binding order observed in the kinetic mechanism of human NMNAT. Extensive crystallization screenings have been carried out in the presence of NMN or PP_i, but no crystals could be obtained. We infer that these unsuccessful trials may be due to NMN- or PP_i-induced conformations that are incompatible with efficient crystal packing.

NMNAT has been recognized as a member of the nucleotidyltransferase α/β-phosphodiesterase superfamily, which includes class I aminoacyl-tRNA synthetase (37), luciferase (38), glycerol-3-phosphate cytidylyltransferase (39), adenylylsulfate-phosphate adenylyltransferase (40, 41), ATP sulfurylase (42), phosphopantetheine adenylyltransferase (PPAT) (43), and pantothenate synthetase (44). These enzymes catalyze the transfer of a nucleotide monophosphate moiety onto different substrates through transition state stabilization without any direct involvement of the chemistry of protein residues in catalysis (18, 43, 45). A peculiar feature of all members of this superfamily is the strict conservation of the (T/H)*X*GH sequence fingerprint with a striking conservation of the second histidine, shown to be involved in substrate binding and transition state stabilization (18, 39, 43). Among nucleotidyltransferase α/β-phosphodiesterases, NMNAT has been reported to be characterized by a wider signature fingerprint consisting of residues G*X*F*X*P*X*(T/H)*XX*H (14). Recently, our group solved the structure of *M. jannaschii* NMNAT in complex with ATP (18), and the structure of *M. thermoautotrophicum* NMNAT in complex with NAD and NMN has also been published (20). A DALI search (46) against the entire Protein Data Bank revealed as the top scores the structures of PPAT (ID code, 1b6t) (43) and *M. jannaschii* NMNAT (ID code,1f9a) (18). PPAT and human NMNAT show 20% sequence identity and can be superposed with an r.m.s.d. of 2.4 Å for 157 Cα pairs, whereas *M. jannaschii* NMNAT and human NMNAT superpose with an r.m.s.d. of 3.0 Å for 146 Cα pairs (20% sequence identity). A structural superposition has also been conducted for the human enzyme and *M. thermoautotrophicum* NMNAT (ID code 1ej2) (20) (showing 18% sequence identity), resulting in an r.m.s.d. of 2.3 Å for 118 Cα pairs.

Based on the these considerations, the active site of human NMNAT has been identified and analyzed (Fig. 4) through sequence and structural comparisons with members of the nucleotidyltransferase α/β-phosphodiesterase superfamily and homology modeling with the *M. jannaschii* and *M. thermoautotrophicum* NMNAT structure in different liganded states. A structural-based sequence alignment revealed only 15 residues strictly conserved in all three NMNAT structures (Fig. 5). Ten of them are fundamental residues for the stability of the NMNAT fold, whereas Gly-15, Pro-19, His-24, Thr-224, and Arg-227 appear to be directly or indirectly involved in ATP recognition and/or catalysis. The strictly conserved residue His-24, part of the ^{21}(T/H)XXH^{24} sequence fingerprint, has been demonstrated to be a key catalytic residue in other nucleotidyltransferase α/β-phosphodiesterases (20, 41) and was proposed as the major protein determinant stabilizing the transition state (18, 43, 45). Therefore, as expected, it is conserved even in human NMNAT. The struc-

```
mjNMNAT      1    LRGFII GRFQPFHKGH LEVIKKIAEE VDEII----- -IGIGSAQKS
mtNMNAT      4    MRGLLV GRMQPFHRGH LQVIKSILEE VDELI----- -ICIGSAQLS
hNMNAT       5  EKTEVVLLAC GSFNPITNMH LRLFELAKDY MNGTGRYTVV KGIISPVGDA
                  .  .   *   *. . * * ..    .  ..           *..   .

mjNMNAT     41  H-TLENPFTA GERILMITQS LKDY---DLT YYPIPIKDIE FNSIWVSYVE
mtNMNAT     44  H-SIRDPFTA GERVMMLTKA LSENGIPASR YYIIPVQDIE CNALWVGHIK
hNMNAT      55  YKKKGLIPAY -HRVIMAELA TKNSKWVEVD TWE----SLQ KEWKETLKVL
                        .    *..*   .   .                ..  .      .

mjNMNAT     87  SLTPPFDI-- --------VY SGNPLVRV-- -----LFEER GYE---VKRP
mtNMNAT     93  MLTPPFDR-- --------VY SGNPLVQR-- -----LFSED GYE---VTAP
hNMNAT     100  RHHQEKLEAS AVPKVKLLCG ADLLESFAVP NLWKSEDITQ IVANYGLICV
                                     .                          .

mjNMNAT    117  EM-------- ---------- ---------- -FNRKEYSGT EIRRRMLNGE
mtNMNAT    123  PL-------- ---------- ---------- -FYRDRYSGT EVRRRMLDDG
hNMNAT     187  TRAGNDAQKF IYESDVLWKH RSNIHVVNEW FAND--ISST KIRRALRRGQ
                                                  *.*  .** .

mjNMNAT    138  KWEHLVPKAV VDVIKEIKGV ERLRKLA
mtNMNAT    144  DWRSLLPESV VEVIDEINGV ERIKHLA
hNMNAT     235  SIRYLVPDLV QEYIEKHNLY SSE
                    *.*  *  . *   .
```

FIG. 5. **A structural-based amino acid sequence alignment of NMNATs.** The sequences of enzymes from *M. jannaschii* (*mjNMNAT*), *M. thermoautotrophicum* (*mtNMNAT*), and human (*hNMNAT*) are shown.

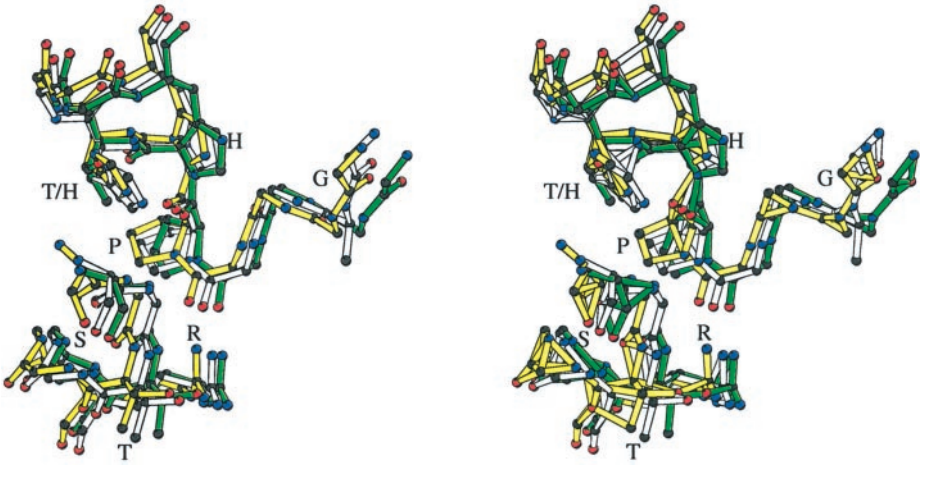

FIG. 6. **Stereo view superposition of the G*XXXP*X(H/T)*XX*H and S*XT-XX*T signature fingerprint of human (*green*), *M. jannaschii* (*yellow*), and *M. thermoautotrophicum* (*white*) NMNATs.** Only the backbones are shown for the non-conserved residues. This figure was generated by using MOLSCRIPT (48).

tural analysis shows that Gly-15 and Pro-19 are needed to properly orient the catalytic relevant His-24 (Fig. 6). Indeed Pro-19 is in the unusual cis conformation in all three NMNAT structures reported to date. Such a conformation determines a peculiar turn of the polypeptide chain resulting in a proper orientation of His-24, whose conformation must be carefully fixed for catalysis (Fig. 6). Despite the fact that it is not strictly conserved, Thr-21 is a key residue for ATP recognition (Figs. 5 and 6). In fact, Thr-21 would contact the ATP β-phosphate, analogously to the His-16 in the *M. jannaschii* NMNAT·ATP complex (18), therefore appearing as an important residue for ATP binding. Moreover, as already reported for glutaminyl-tRNA synthetase (47), PPAT (43), and *M. jannaschii* NMNAT (18), the main chain nitrogen atom of Thr-21 is hydrogen-bonded to the δ-nitrogen of His-24, which is therefore neutral with a proton localized on its ϵ-nitrogen. Such a remarkable conservation of the hydrogen-bonding scheme for the residues (part of the (T/H)*XX*H motif) strongly supports the notation of a relevant role in catalysis for the second conserved histidine supposed to stabilize the transition state intermediate. With respect to ATP binding, as much as the role played by Thr-224 and Arg-227 appears to be important, both are strictly conserved in all NMNATs (Fig. 5). The two residues are part of the ^{222}S*X*T*XX*R^{227} sequence, which is structurally conserved in all NMNATs (Figs. 5 and 6). Both the threonine and arginine residues were reported to stabilize the ATP γ-phosphate in the structure of the *M. jannaschii* NMNAT·ATP complex (18). Moreover, the S*X*-T*XX*R motif is localized at the N terminus of the H8 helix (Figs. 1 and 4), a conserved secondary structural element in NMNATs, which was suggested to participate in ATP recognition through the interaction of its dipole with the ATP β-phosphate in the *M. jannaschii*·ATP complex (18). On the other hand, none of the residues contacting the ATP α- and β-phosphates in the *M. jannaschii* NMNAT·ATP complex are conserved in the human enzyme. Particularly interesting is the absence in the human enzyme of a highly conserved arginine residue contacting the ATP β-phosphate in all nucleotidyltransferases, which was suggested to be a key residue for ATP recognition in nucleotidyltransferases (18, 39, 43, 47). Based on the structure of the free form of human NMNAT, the unusual ATP conformation observed in the *M. jannaschii* structure (18) appear to be mainly dictated by the strong interactions observed between ATP γ-phosphate and the conserved threonine and arginine protein residues (Thr-224 and Arg-227 in the human enzyme). Therefore, the conserved residues (part of the T*XX*H and S*X*T*XX*R motifs) could represent the minimal and essential structural requirement for ATP recognition in all NMNATs. However, we cannot rule out the possibility of an ATP-induced conformational change that could bring into place other protein residues relevant for nucleotide recognition. Altogether, we identified two strictly structurally conserved sequence fingerprints in all NMNATs, G*XXX*P*X*(T/H)*XX*H and S*X*T*XX*R (Figs. 5 and 6), both featuring the ATP binding site. Moreover, we propose as the universal sequence signature fingerprint for α/β-nucleotidyltransferases the (T/H)*XX*H motif, the glycine residue being included previously into the signature ((T/H)*X*GH) but not present in human NMNAT and not essential to maintain the conformation adopted by the motif (Fig. 6).

Quite surprisingly, none of the residues reported to bind NMN in the *M. thermoautotrophicum* NMNAT (20) are observed in the structure of the human enzyme, making any proposal about the NMN binding mode poorly reliable. In particular, neither Trp-87 nor Asn-84, which have been recognized as key residues in the recognition of NMN in *M. thermoautotrophicum* NMNAT (20), are observed in an equivalent position in human NMNAT. In the human enzyme, two residues, Trp-169 and Glu-94, are located in close proximity to the expected NMN binding site and could be involved in the binding of the nicotinic moiety of NMN (Fig. 4). However, such a possibility would again require a conformational change induced by substrate binding, properly building the NMN binding site. In fact, a crude homology modeling based on the structural superposition with *M. jannaschii* NMNAT-ATP and *M. thermoautotrophicum* NMNAT·NAD complexes, aimed at the definition of NMN and ATP binding sites, reveals a number of serious steric collisions at both sites. Such observations support the hypothesis of a conformational change induced by substrate binding, resulting in the proper assembly of the enzyme active site.

Acknowledgments—We thank Profs. Andrea Mattevi (University of Pavia), Martino Bolognesi (University of Genova), and Nadia Raffaelli (University of Ancona) for many helpful and stimulating discussions. We thank the staff at the European Synchrotron Radiation Facility in Grenoble, France for help during data collection.

REFERENCES

1. Lee, H. C. (1997) *Physiol. Rev.* **77,** 1133–1164
2. Patel, S., Churchill, G. C., and Gallione, A. (2001) *Trends Biochem. Sci.* **26,** 482–489
3. De Murcia, G., and Shall, S. (2001) in *From DNA Damage and Stress Signaling to Cell Death: Poly ADP-Ribosylation Reactions*, Oxford University Press Inc., New York
4. Okazaki, I. J., and Moss, J. (1996) *Adv. Pharmacol.* **35,** 247–280
5. Lin, S. J., Defossez, P. A., and Guarante, L. (2000) *Science* **289,** 2126–2128
6. Smith, J. S., Brachmann, C. B., Celic, I., Kenna, M. A., Muhammad, S., Starai, V. J., Avalos, J. L., Escalante-Semerena, J. C., Grubmeyer, C., Wolberger, C., and Boeke, J. D. (2000) *Proc. Natl. Acad. Sci. U. S. A.* **97,** 6658–6663
7. Hughes, K. T., Lakida, D. Roth, J. R., and Olivera, B. M. (1983) *J. Bacteriol.* **155,** 213–221
8. Magni, G., Amici, A., Emanuelli, M., Raffaelli, N., and Ruggieri, S. (1999) *Adv. Enzymol. Relat. Areas Mol. Biol.* **73,** 135–182
9. Lowe, G and Tansley, G. (1983) *Eur. J. Biochem.* **132,** 117–120
10. Di Lisa, F., and Ziegler, M. (2001) *FEBS Lett.* **492,** 4–8
11. Balducci, E., Emanuelli, M. Magni, G., Raffaelli, N., Ruggieri, S., Vita, A., and Natalini, P. (1992) *Biochem. Biophys. Res. Commun.* **189,** 1275–1279
12. Schweiger, M., Hennig, K., Lerner, F., Niere, M., Hirsch-Kauffmann, M., Specht, T., Weise, C., Oei, S. L., and Ziegler, M. (2001) *FEBS Lett.* **492,** 95–100
13. Emanuelli, M. Raffaelli, N., Amici, A., Balducci, E., Natalini, P., Ruggieri, S., and Magni G. (1995) *Biochem. Pharmacol.* **49,** 575–579
14. Emanuelli, M., Carnevali, F., Saccucci, F., Pierella, F., Amici, A., Raffaelli, N., and Magni, G. (2001) *J. Biol. Chem.* **276,** 406–412
15. Jayaram, H. N., Pillwein, K., Lui, M. S., Faderan, M. A., and Weber, G. (1986) *Biochem. Pharmacol.* **35,** 587–593
16. Jayaram, H. N., Cooney, D. A., and Grusch, M. (1999) *Curr. Med. Chem.* **6,** 561–574
17. Boulton, S., Kyle, S, and Durkacz B. W. (1997) *Br. J. Cancer* **76,** 845–851
18. D'Angelo, I., Raffaelli, N., Dabusti, V., Lorenzi, T., Magni, G., and Rizzi, M. (2000) *Structure* **8,** 993–1004
19. Bork, P., Holm, L., Koonin, E., and Sander C. (1995) *Proteins Struct. Funct. Genet.* **22,** 259–266
20. Saridakis, V., Christendat, D., Kimber, M. S., Dharamsi, A, Edwards, A. M., and Pai, E. F. (2001) *J. Biol. Chem.* **276,** 7225–7232
21. Rizzi, M., Nessi, C., Mattevi, A., Coda, A., Bolognesi, M., and Galizzi, A. (1996) *EMBO J.* **15,** 5125–5134
22. Mattevi, A., Tedeschi, G., Bacchella, L., Coda, A., Negri, A., and Ronchi, S. (1999) *Structure* **7,** 745–756
23. Leslie, A. G. W. (1992) *Joint CCP4 and ESF-EACMB Newsletter Protein Crystallography*, No. 26, SERC Daresbury Laboratory, Warrington, UK
24. Collaborative Computational Project Number 4 (1994) *Acta Crystallogr. Sect. D Biol. Crystallogr.,* **50,** D760–D767
25. Sheldrick, G. M. (1991) in *Proceedings of the CCP4 Study Weekend: Isomorphous Replacement and Anomalous Scattering 25–26 January 1991* (Wolf, W., Evans, P. R., and Leslie, A. G. W., eds), pp. 23–38, SERC Daresbury Laboratory, Warrington, UK
26. Otwinowski, Z. (1991) in *Proceedings of the CCP4 Study Weekend 25–26 January 1991* (Wolf, W., Evans, P. R., and Leslie, A. G. W., eds), pp. 80–86, SERC Daresbury Laboratory, Warrington, UK
27. Navaza, J. (1994) *Acta Crystallogr. Sect. A* **50,** A157–A163
28. Tong, L., and Rossmann, M. G. (1990) *Acta Crystallogr. Sect. A* **46,** A783–A792
29. Cowtan, K. D., and Main, P. (1996) *Acta Crystallogr. Sect. D Biol. Crystallogr.* **52,** D43–D48
30. Jones, T. A., Zou, J. Y., Cowan, S. W., and Kjeldgaard, M. (1991) *Acta Crystallogr. Sect. A* **47,** A110–A119
31. Murshudov, G. N., Vagin, A. A., and Dodson, E. J. (1997) *Acta Crystallogr. Sect. D Biol. Crystallogr.* **53,** D240–D255
32. Brünger, A. T. (1992) *Nature* **355,** 472–474
33. Laskowski, R. A., MacArthur, M. W., Moss, D. S., and Thornton, J. M. (1993)

J. Appl. Crystallogr. **26,** 283–291
34. Schweiger, M., Lerner, F., Hennig, K., Niere, M., Hirsch-Kauffmann M., Oei, S. L., and Ziegler, M. (2001) in *Targeting ADP-Ribosylation for Development of New Therapies*, p. 89,13th International Symposium on ADP-Ribosylation, June 8–11, New York, NY
35. Ruggieri, S., Gregori, L., Natalini, P., Vita, A., Emanuelli, M., Raffaelli, N., and Magni G. (1990) *Biochemistry* **29,** 2501–2506
36. Emanuelli, M., Natalini, P., Raffaelli, N., Ruggieri, S., Vita, A., and Magni, G. (1992) *Arch. Biochem. Biophys.* **298,** 29–34
37. Cusack, S. (1997) *Curr. Opin. Struct. Biol.* **7,** 881–889
38. Conti, E., Franks, N. P., and Brick, P. (1996) *Structure* **4,** 287–298
39. Weber, C. H., Park, Y. S., Sanker, S., Kent, C., and Ludwig, M. L. (1999) *Structure* **7,** 1113–1124
40. Bruser, T., Selmer, T., and Dahl, C. (2000) *J. Biol. Chem.* **275,** 1691–1698
41. Venkatachalam, K. V., Fuda, H., Koonin, E. V., and Strott, C. A. (1999) *J. Biol. Chem.* **274,** 2601–2604
42. Ulrich, T. C., Blaesse, M., and Huber, R. (2001) *EMBO J.* **20,** 316–329
43. Izard, T., and Geerlof, A. (1999) *EMBO J.* **18,** 2021–2030
44. van Delft F., Lewendon, A., Dhanaraj, V., Blundell, T. L., Abell, C., and Smith, A. G. (2001) *Structure* **9,** 439–450
45. Fersth, A. R. (1987) *Biochemistry* **26,** 8031–8037
46. Holm, L., and Sander, C. (1997) *Structure* **5,** 165–171
47. Perona, J. J., Rould, M., and Steitz, T. A. (1993) *Biochemistry* **32,** 8758–8771
48. Kraulis, P. J. (1991) *J. Appl. Crystallogr.* **24,** 946–950

Structure of Human NMN Adenylyltransferase: A KEY NUCLEAR ENZYME FOR NAD HOMEOSTASIS

Silvia Garavaglia, Igor D'Angelo, Monica Emanuelli, Francesco Carnevali, Francesca Pierella, Giulio Magni and Menico Rizzi

J. Biol. Chem. 2002, 277:8524-8530.
doi: 10.1074/jbc.M111589200 originally published online December 19, 2001
